PHENOMENOLOGICAL CHARACTERIZATION OF BACTERIORHODOPSIN–D85N PHOTOCYCLE

Doğan A. Timuçin and John D. Downie

NASA Ames Research Center, M.S. 269-3, Moffett field, CA 94035

Abstract

An operational characterization of the molecular photocycle of a genetic variant of bacteriorhodopsin, BR–D85N, is presented. Steady-state bleach spectra and pump–probe absorbance data are obtained with thick hydrated films containing BR–D85N embedded in a gelatin host. Simple two- and three-state models are used to analyze the photocycle dynamics and extract relevant information such as pure-state absorption spectra, photochemical-transition quantum efficiencies, and thermal lifetimes of dominant states appearing in the photocycle, the knowledge of which should facilitate the analysis and design of optical applications based on this photochromic medium. The remarkable characteristics of this material and their implications from the viewpoint of optical data storage and processing are discussed.

OCIS codes

090.2900, 160.2900, 210.4810, 230.6120, 260.5130, 300.1030

Phenomenological characterization of bacteriorhodopsin–D85N photocycle

1 Introduction

Bacteriorhodopsin (BR) is a chromophoric protein found in the crystalline purple membrane (PM) of *Halobacterium salinarium*, and acts as a light-driven proton pump aiding in the organism's photosynthetic ATP production in oxygen-deficient environments where aerobic survival is not possible. Photochromic films incorporating BR and its numerous chemical and genetic variants have been used with considerable success in many optical data storage and processing applications in the past; several excellent review articles discuss the biophysical and biochemical structure and function of BR as well as its technical applications.[1] In most (if not all) optical applications, the photochromic nature of BR is exploited to induce a suitable absorption and concomitant refractive-index change within the volume of the film by creating a spatiotemporally varying population difference between a sufficiently long-lived intermediate state in the photocycle and the thermally-stable "ground" *B* state of the molecule, thus accomplishing the desired storage or processing of information carried by optical waves.[2]

One of the most attractive genetic mutants of BR for optical data storage is D85N, which belongs to a class of BR material referred to as blue membrane (BM) and is grown by means of the substitution Asp-85 $\rightarrow$ Asn in the 248-amino-acid polypeptide chain that forms a 7-segment α-helical pocket around the all–*trans* retinal chromophore.[3] This site-specific mutagenesis effectively blocks the proton translocation pathway inside the pocket, hindering the normal completion of the molecular photocycle. Thus, unlike the naturally occurring PM (wild-type) BR and other popular variants such as D96N, the photocycle of D85N contains an extremely long-lived intermediate *P* state that offers the capability of near-permanent data storage.

The photophysics and photochemistry of D85N, as well as those of the other BM forms of BR that exhibit similar photocycle structures and spectral properties, namely the acidified BM and the deionized BM, have been studied extensively.[4–13] Our goal here is to provide, based on steady-state bleach spectra and pump–probe absorbance data, an operational characterization of the BR–D85N photocycle, concentrating on the salient features of this material pertinent to optical data storage and processing applications. Thus, as the adjective "phenomenological" in the title implies, we are not seeking to catalog the detailed photochemical properties of pure D85N, which can largely be found in the BR photochemistry literature cited above, but instead attempting to describe its relevant optical characteristics when mixed with other ingredients and cast in the form of a thick high-optical-quality medium. The choice of working with steady-state, rather than pulsed, excitation was also made in this spirit; that is, we intend to study the material response under this condition since this is the way we envision the medium to be used in storage and processing applications. Thus, for instance, whereas pulsed excitation and ultrafast time-resolved spectroscopy would be indispensable in extracting the quantum efficiency of the primary photoevent $B \rightarrow K$, this is not a relevant quantity for the applications of interest to us as the K intermediate plays no significant role in this context. Instead, the critical quantity for us is the "effective" quantum efficiency of the key transition $B \rightarrow P$, which is best (or at least just as easily) extracted from steady-state bleach spectra.

The BR films used in this study were produced by Bend Research, Inc., through a proprietary film fabrication process developed during the course of several NASA-funded SBIR contracts. Briefly, the genetic D85N material, grown by Prof. George Rayfield at the University of Oregon, was mixed with gelatin, glycerol, and water at neutral pH, cast in two layers between plane-parallel glass plates, and sealed with UV-cured epoxy, forming a high optical-quality film.

Although we experimented with films of various size (1–2″ in diameter), thickness (100 μm–2 mm), and optical density (1.8–3.5 OD), for the sake of consistency we shall present data obtained with a single film in this paper, with the results obviously being representative of the whole batch.

2 Two-state model

Two-state models have been widely, and successfully, used in the past to explain the optical characteristics of BR films;[14] it is therefore tempting to start our consideration of the BR–D85N photocycle with the model shown in Fig. 1. Only photo-induced molecular transitions are allowed in this model, with possible thermal relaxation of the *P* state ruled out for the time being, as it has been generally assumed to be stable at room temperatures.

A Theoretical development

The photochemical transition rate from state q to state p is designated γ_{pq}^{P} and can be expressed in the form[2]

$$\gamma_{pq}^{P}(\lambda_0;\mathbf{r},t) = \ln 10\,\phi_{pq}(\lambda_0)\frac{A_q(\lambda_0)}{N_0 d}\frac{\lambda_0}{hc_0}I(\mathbf{r},t) \equiv \rho_{pq}(\lambda_0)\,I(\mathbf{r},t), \tag{2-1}$$

where $\phi_{pq}(\lambda)$ is the quantum efficiency of the $q \to p$ transition, $A_q(\lambda)$ is the absorption spectrum of the q state, λ_0 is the (vacuum) wavelength of the optical excitation, N_0 is the volume number density of BR molecules in the film, d is the film thickness, h and c_0 denote

Planck's constant and the (vacuum) speed of light, respectively, and $I(\mathbf{r},t)$ is the space- and time-varying intensity of the field inside the film.

Clearly, the absorption spectra of the various molecular states of BR critically affect the optical properties of the film. Now, the pure *B*-state spectrum $A_B(\lambda)$ can be readily obtained via a spectrophotometer measurement performed on the unexposed film (in which all BR molecules are in the *B* state). Since it is not possible to fully populate the *P* state, however, the pure *P*-state spectrum $A_P(\lambda)$ cannot be obtained directly, and must be extracted from the measured absorption spectrum of the exposed film, which is generally a linear superposition of A_B and A_P with time-varying weights, viz.

$$A(\lambda;t) = \frac{1}{d}\int_0^d \left[n_B(z,t)A_B(\lambda) + n_P(z,t)A_P(\lambda) \right] \mathrm{d}z, \tag{2-2}$$

where $n_q(\mathbf{r},t)$ denotes the fractional population density of the q state, related to the volume number density $N_q(\mathbf{r},t)$ of the q-state molecules in the obvious fashion as $n_q = N_q / N_0$, and we assumed for concreteness and simplicity that the film is bleached by a normally incident plane wave, hence resulting in only a z dependence for the intensity and population distributions inside the film. Noting that $n_B + n_P = 1$, the rate equation governing the *B*-state population can be written down readily as

$$\frac{\partial n_B}{\partial t} = -\left[\rho_{PB}(\lambda_0) + \rho_{BP}(\lambda_0) \right] I\, n_B + \rho_{BP}(\lambda_0)\, I, \tag{2-3}$$

while, in accord with the Lambert–Beer law, the optical intensity evolves as

$$\frac{\partial I}{\partial z} = -\frac{\ln 10}{d}\left\{\left[A_B(\lambda_0) - A_P(\lambda_0)\right] n_B + A_P(\lambda_0)\right\} I. \tag{2-4}$$

Unfortunately, the coupled system of Eqs. (2-3 and 4) cannot be solved generally for $n_B(z,t)$ and $I(z,t)$ in closed form, hindering analytical progress with Eq. (2-2). Matters are greatly simplified, however, if the film is bleached to steady-state conditions ($t \to \infty$), for which case we readily find from Eq. (2-3) by setting $\partial/\partial t \equiv 0$ that

$$n_B^{ss_0} = \frac{\rho_{BP}(\lambda_0)}{\rho_{PB}(\lambda_0) + \rho_{BP}(\lambda_0)} = \frac{1}{1 + \Phi(\lambda_0)\frac{A_B(\lambda_0)}{A_P(\lambda_0)}}, \tag{2-5}$$

where the superscript ss_0 denotes steady state reached with bleaching wavelength λ_0, and $\Phi \equiv \phi_{PB}/\phi_{BP}$ is the ratio of forward- to backward-transition quantum efficiencies.

With constant steady-state population densities throughout the depth of the film, implying an exponentially decaying steady-state intensity distribution inside the film [cf. Eq. (2-4)], the integration in Eq. (2-2) is now trivial, and the steady-state absorption spectrum of the film can be written down readily as

$$A^{ss_0}(\lambda) = n_B^{ss_0} A_B(\lambda) + n_P^{ss_0} A_P(\lambda) = \frac{A_B(\lambda) + \Phi(\lambda_0)\frac{A_B(\lambda_0)}{A_P(\lambda_0)} A_P(\lambda)}{1 + \Phi(\lambda_0)\frac{A_B(\lambda_0)}{A_P(\lambda_0)}}, \tag{2-6}$$

where we substituted in Eq. (2-5) and made use of $n_P = 1 - n_B$. Evaluating Eq. (2-6) at $\lambda = \lambda_0$ first, we find the hitherto unknown quantity

$$A_P(\lambda_0) = \frac{\Phi(\lambda_0) A_B(\lambda_0) A^{ss_0}(\lambda_0)}{\left[1 + \Phi(\lambda_0)\right] A_B(\lambda_0) - A^{ss_0}(\lambda_0)}. \tag{2-7}$$

We then solve for $A_P(\lambda)$ from Eq. (2-6), obtaining, with the help of Eq. (2-7), our final result:

$$A_P(\lambda) = \frac{\left[1 + \Phi(\lambda_0)\right] A_B(\lambda_0) A^{ss_0}(\lambda) - A^{ss_0}(\lambda_0) A_B(\lambda)}{\left[1 + \Phi(\lambda_0)\right] A_B(\lambda_0) - A^{ss_0}(\lambda_0)}. \tag{2-8}$$

We have thus succeeded in expressing the pure *P*-state spectrum A_P entirely in terms of the experimentally measured *B*- and steady-state spectra A_B and A^{ss}. The parameter $\Phi(\lambda_0)$, however, remains unknown except for the obvious condition $0 < \Phi < \infty$ imposed by its very definition; two different bounds can be derived for this quantity, as described presently. The first, and the obvious, requirement is that of positive-semidefiniteness for the calculated pure *P*-state spectrum; i.e., $A_P(\lambda) \geq 0 \ \ \forall \lambda$, which yields the lower bound

$$\Phi(\lambda_0) \geq \frac{A^{ss_0}(\lambda_0)}{A_B(\lambda_0)} \sup_{\lambda} \left[\frac{A_B(\lambda)}{A^{ss_0}(\lambda)} \right] - 1. \tag{2-9}$$

A second, and perhaps less evident, requirement can now be imposed upon Eq. (2-8) by noting that, since the *P* state can be only partially populated, at wavelengths above the (quasi-)isosbestic

point [cf. Fig. 3] the calculated pure *P*-state spectrum must lie entirely below the measured steady-state spectrum. A moment's reflection reveals that it is necessary to introduce a second bleaching wavelength $\lambda_1 > \lambda_0$ to be able to bound $\Phi(\lambda_0)$ from above via this argument, and thus we have the requirement $A_P(\lambda) \le A^{ss_1}(\lambda) \quad \forall \lambda \ge \lambda_{iso}$, which leads to the upper bound ($\Lambda = \{\lambda \,|\, \lambda \ge \lambda_{iso}\}$)

$$\Phi(\lambda_0) \le \frac{A^{ss_0}(\lambda_0)}{A_B(\lambda_0)} \inf_{\Lambda} \left[\frac{A_B(\lambda) - A^{ss_1}(\lambda)}{A^{ss_0}(\lambda) - A^{ss_1}(\lambda)} \right] - 1. \tag{2-10}$$

B Experimental results

In order to calculate the pure *P*-state spectrum within the framework of this two-state photocycle model, a 2-mm thick BR–D85N film, whose initial (i.e., pure *B*-state) absorption spectrum is shown in Fig. 2 (initial optical density at 600 nm of $iOD_{600} \cong 3$),[15] was bleached to steady state by a collimated beam through a 6-mm × 9-mm aperture, first with a 633-nm He–Ne laser, and then with two separate diode lasers operating at 670 nm and 690 nm. During exposure, the time evolution of the film transmittance (at the bleaching wavelength) was monitored by means of a photodetector to ensure the attainment of steady-state conditions. Once in steady state, the film was removed from the bleaching beam and promptly placed in the spectrophotometer for measurement of its absorption spectrum. The bleached area was irradiated after each exposure with a 442-nm He–Cd laser to restore the film to its initial condition before the next experiment.

Fig. 3 shows the steady-state absorption spectra of the film for these three bleaching

wavelengths. The most immediate observation to be made is that larger fractions of BR molecules seem to be excited into the *P* state with bleaching wavelengths that are deeper into the red part of the spectrum. Table 1 summarizes the results of the quantitative analysis based on these measurements regarding the value of the quantum-efficiency ratio. We note firstly that, owing to $\lambda_0 > \lambda_{iso}$ (as is required for photo-bleaching), the right-hand side of Eq. (2-9) is strictly positive, thus providing useful lower bounds on $\Phi(\lambda_0)$ for all three bleaching wavelengths. We observe also that the further apart the two bleaching wavelengths (λ_0 and λ_1) are, the tighter the upper bound in Eq. (2-10) becomes, asymptotically approaching from above (but never reaching) that of Eq. (2-9); indeed, as seen in Table 1 for the case of λ_0 = 633 nm, the upper bound on $\Phi(\lambda_0)$ obtained for λ_1 = 690 nm is approximately three times smaller than that for λ_1 = 670 nm. The distressing observation here, though, is that the lower and upper bounds for any given bleaching wavelength λ_0 are roughly two orders of magnitude apart, hence failing to provide a narrow window for the estimation of $\Phi(\lambda_0)$. We are thus forced to resort to a somewhat arbitrary method of estimation, and we found that, as a rule of thumb, the geometric mean of the lower and upper bounds at λ_0 provides a fairly satisfactory value for $\Phi(\lambda_0)$. Since we have two distinct upper bounds for λ_0 = 633 nm, we show the arithmetic mean of the two corresponding geometric means in this case, which comes out remarkably close to the experimentally determined value $\frac{1}{55} \cong 0.0182$ quoted in the literature for 630-nm excitation of (aqueous) deionized BM.[7] Also, a finite upper bound on $\Phi(\lambda_0)$ for λ_0 = 690 nm cannot be obtained due to the lack of a bleaching source with a longer wavelength, and it was found that five times the corresponding lower bound gives a good estimate for the quantum-efficiency ratio in this case. As a check for the soundness of our estimation scheme, we find, by linear interpolation based on

the three values shown in Table 1, the value of $\Phi(\lambda_0)$ at λ_0 = 647 nm to be 0.0337, which is within the experimentally determined range of $\frac{1}{33\pm5} \cong (0.0263, 0.0357)$ for 647-nm excitation of (dried) deionized BM.[13]

We should stress that the quantum-efficiency ratio figures listed in Table 1 are designated as typical values due to the *ad hoc* manner in which they were estimated, and are merely meant to exhibit the relative (order-of-magnitude) variation in $\Phi(\lambda_0)$ as a function of the bleaching wavelength. Despite this inevitable lack of precision, it is safe to say that (within the spectral region of interest to us) $\Phi(\lambda)$ seems to increase, apparently linearly and rather dramatically, with increasing wavelength. Obviously, this trend may result from an increase in ϕ_{PB} or a decrease in ϕ_{BP} (while ϕ_{BP} or ϕ_{PB}, respectively, remain relatively constant), or both taking place simultaneously. A more detailed understanding of this behavior requires a complete molecular-dynamics simulation at the quantum-chemical level, aided by ultrafast time-resolved absorption spectroscopy, to map out the different ground- and excited-state energy surfaces and the associated (radiative and nonradiative) transitions in BR–D85N, which is beyond the scope of the present effort.[13,16]

With the value of $\Phi(\lambda_0)$ thus determined, albeit approximately, we turn to evaluate the pure *P*-state spectrum. As $A_P(\lambda)$ represents an inherent characteristic of the material, data for different bleaching wavelengths should all yield the same result through Eq. (2-8); in fact, this requirement was the primary criterion used above in determining the values of $\Phi(\lambda_0)$. The calculated pure *P*-state spectra for λ_0 = 633 nm, 670 nm, and 690 nm therefore turn out to be nearly indiscernible, and Fig. 4 shows the one obtained with 670-nm data, which has the smoothest tail roll-off (i.e., minimal residual spectral contribution from the *B* state) and was therefore judged the most realistic. The steady-state population densities of the two states are

also shown in Table 1 based on the values of $\Phi(\lambda_0)$ for the three bleaching wavelengths, confirming our earlier qualitative observation that longer bleaching wavelengths more fully excite the BR molecules from the *B* state to the *P* state.

3 Three-state model

A Motivation

Toward assessing the thermal stability of the BR–D85N molecules in *P* state, a pump–probe experiment was performed next whereby the film was first bleached to steady state by a pump beam approximately 10 mW in power,[17] and then the film absorbance was monitored as a function of time by means of a weak intermittent probe beam, derived from the pump beam with a shutter and a 3-OD attenuation provided by a neutral-density filter. (The need for the pump and probe beams to be of the same wavelength will become evident in the course of the ensuing analysis.) The first 10-minute segment of 633-nm probe absorbance data is given in Fig. 5, which not only shows that the film absorbance (at the pump–probe wavelength) changes in time once the pump beam is turned off (at $t = 0$), indicating a rearrangement of the steady-state population densities through dark (i.e., thermal) processes, but it also reveals that this kinetic behavior cannot be modeled adequately with a single exponential (which would presumably represent the thermal decay of the *P*-state molecules), hinting at the presence of one or more additional intermediate states in the photocycle.[18]

Further supporting evidence for this is provided by Fig. 6, which shows the evolution of the entire absorption spectrum of the film as a function of time after having been bleached to steady state by a 633-nm source, with $t = 0$ again marking the instant the pump beam is turned

off. (To facilitate comparison, we mention that the spectra shown in Fig. 3 were all measured 30 seconds after the pump beams were turned off; i.e., the curve labeled “633 nm” in Fig. 3 and the one labeled “30 sec” in fig. 6 are the same.) The key observation here is that although the *P*-state peak at 490 nm appears to be declining very slowly, there is a substantial rise in the *B*-state peak at 600 nm early on (i.e., within the first 5 minutes). This can be accounted for by the thermal decay (back to *B*) of a third short-lived (compared to *P*) state whose absorbance at 633 nm is less than that of the *B* state.

The same probe-absorbance and time-resolved spectral measurements were then repeated with a 670-nm source (data not shown); although a similar trend was observed here as well, the increase in film absorbance in the red part of the spectrum and over the same period of time was much less prominent in this case. This, in turn, leads to one or both of the following inferences: (1) the steady-state population of this third state attained under 670-nm excitation is smaller than that for 633-nm excitation, and (2) its absorbance at 670 nm is smaller than its value at 633 nm, implying that the peak of its absorption spectrum is likely to be somewhere between those of the *B* and *P* states.

These observations compel us to consider the *L* state, known to be the dominant intermediate state in the BM photocycle,[6,9–11] as the most likely candidate for the heretofore unidentified third state. Since the *P* and *L* states have 9–*cis* and 13–*cis* retinal configurations, respectively, the proposed three-state photocycle model shown in fig. 7 features a bifurcated structure with two competing photocycles $B \leftrightarrow P$ and $B \leftrightarrow L$. (The well-known precursor of *L*, the *K* state, is not included in this model as it is supposed to be very short-lived.[10–12])

B Theoretical development

The population densities of the three states here evolve according to[2]

$$\frac{\partial}{\partial t}\begin{bmatrix} n_B \\ n_L \\ n_P \end{bmatrix} = \begin{bmatrix} -\gamma_{LB}^P - \gamma_{PB}^P & \gamma_{BL}^P + \gamma_{BL}^T & \gamma_{BP}^P + \gamma_{BP}^T \\ \gamma_{LB}^P & -\gamma_{BL}^P - \gamma_{BL}^T & 0 \\ \gamma_{PB}^P & 0 & -\gamma_{BP}^P - \gamma_{BP}^T \end{bmatrix} \cdot \begin{bmatrix} n_B \\ n_L \\ n_P \end{bmatrix}, \tag{3-1}$$

where γ_{pq}^T designates the thermal relaxation rate from state q to state p. Due to the time dependence of the photochemical transition rates γ_{pq}^P [cf. Eq. (2-1)], a closed-form solution cannot be written down for Eq. (3-1); fortunately, however, we shall be interested in two separate experimental regimes in the sequel, for which Eq. (3-1) takes simpler forms, as detailed below.

With a sufficiently strong pump beam of wavelength λ_0 illuminating the film, one can safely assume that $\gamma_{Bq}^T << \gamma_{Bq}^P$, thus enabling the elimination of the thermal decay rates from Eq. (3-1); that this is indeed justifiable will be established subsequently. After adequate exposure, the film reaches steady state, and the corresponding molecular population densities can be found readily by setting the left-hand side of Eq. (3-1) equal to zero, leading to

$$\begin{bmatrix} n_B^{ss_0} \\ n_L^{ss_0} \\ n_P^{ss_0} \end{bmatrix} = \frac{1}{1 + \Phi_L(\lambda_0)\frac{A_B(\lambda_0)}{A_L(\lambda_0)} + \Phi_P(\lambda_0)\frac{A_B(\lambda_0)}{A_P(\lambda_0)}} \begin{bmatrix} 1 \\ \Phi_L(\lambda_0)\frac{A_B(\lambda_0)}{A_L(\lambda_0)} \\ \Phi_P(\lambda_0)\frac{A_B(\lambda_0)}{A_P(\lambda_0)} \end{bmatrix}, \tag{3-2}$$

where $\Phi_q \equiv \phi_{qB} / \phi_{Bq}$ are the ratios of forward- to backward-transition quantum efficiencies between states B and $q = L, P$.

When the pump beam is turned off, which is assumed for convenience to occur at $t = 0$, the molecules in the L and P states are free to relax thermally, thus leading to a redistribution of BR molecules among the three states. Since we now have $I = 0$, the photochemical transition rates in Eq. (3-1) are identically zero, and thus, using the steady-state solution Eq. (3-2) as the initial condition, the population densities are found to rearrange themselves as

$$\begin{bmatrix} n_B(t) \\ n_L(t) \\ n_P(t) \end{bmatrix} = \begin{bmatrix} 1 - n_L^{ss_0} \exp\left(-\gamma_{BL}^T t\right) - n_P^{ss_0} \exp\left(-\gamma_{BP}^T t\right) \\ n_L^{ss_0} \exp\left(-\gamma_{BL}^T t\right) \\ n_P^{ss_0} \exp\left(-\gamma_{BP}^T t\right) \end{bmatrix} \tag{3-3}$$

for $t \geq 0$, where we made use of the fact that $n_B + n_L + n_P = 1$. The film absorbance seen by the probe beam at λ_0 can thus be written in the form

$$\begin{aligned} A(\lambda_0; t) &= \begin{bmatrix} A_B(\lambda_0) & A_L(\lambda_0) & A_P(\lambda_0) \end{bmatrix} \cdot \begin{bmatrix} n_B(t) \\ n_L(t) \\ n_P(t) \end{bmatrix} \\ &= A_B(\lambda_0) - \Delta A_L(\lambda_0) \exp\left(-\gamma_{BL}^T t\right) - \Delta A_P(\lambda_0) \exp\left(-\gamma_{BP}^T t\right), \end{aligned} \tag{3-4}$$

$t \geq 0$, where we implicitly defined

$$\begin{aligned} \Delta A_L(\lambda_0) &= n_L^{ss_0} \left[A_B(\lambda_0) - A_L(\lambda_0) \right], \\ \Delta A_P(\lambda_0) &= n_P^{ss_0} \left[A_B(\lambda_0) - A_P(\lambda_0) \right], \end{aligned} \tag{3-5}$$

which give the change in film absorbance due to L- and P-state decay, respectively. Inserting

from Eq. (3-2) into Eq. (3-5) and solving simultaneously, we obtain

$$A_L(\lambda_0) = \frac{A_B(\lambda_0)\left[A_B(\lambda_0) - \Delta A_L(\lambda_0) - \Delta A_P(\lambda_0)\right]\Phi_L(\lambda_0)}{\Delta A_L(\lambda_0)\left[1+\Phi_P(\lambda_0)\right] + \Phi_L(\lambda_0)\left[A_B(\lambda_0) - \Delta A_P(\lambda_0)\right]},$$
$$A_P(\lambda_0) = \frac{A_B(\lambda_0)\left[A_B(\lambda_0) - \Delta A_L(\lambda_0) - \Delta A_P(\lambda_0)\right]\Phi_P(\lambda_0)}{\Delta A_P(\lambda_0)\left[1+\Phi_L(\lambda_0)\right] + \Phi_P(\lambda_0)\left[A_B(\lambda_0) - \Delta A_L(\lambda_0)\right]}, \tag{3-6}$$

and substituting these expressions back into Eq. (3-2), we also find

$$n_L^{ss_0} = \frac{\Delta A_L(\lambda_0)\left[1+\Phi_P(\lambda_0)\right] + \Phi_L(\lambda_0)\left[A_B(\lambda_0) - \Delta A_P(\lambda_0)\right]}{A_B(\lambda_0)\left[1+\Phi_L(\lambda_0)+\Phi_P(\lambda_0)\right]},$$
$$n_P^{ss_0} = \frac{\Delta A_P(\lambda_0)\left[1+\Phi_L(\lambda_0)\right] + \Phi_P(\lambda_0)\left[A_B(\lambda_0) - \Delta A_L(\lambda_0)\right]}{A_B(\lambda_0)\left[1+\Phi_L(\lambda_0)+\Phi_P(\lambda_0)\right]}. \tag{3-7}$$

finally, as a direct generalization of Eq. (3-4), we express the entire (transient) absorption spectrum of the film as a function of time as

$$A(\lambda;t) = A_B(\lambda)\left[1 - n_L^{ss_0}\exp\left(-\gamma_{BL}^T t\right) - n_P^{ss_0}\exp\left(-\gamma_{BP}^T t\right)\right] + n_L^{ss_0}A_L(\lambda)\exp\left(-\gamma_{BL}^T t\right) + n_P^{ss_0}A_P(\lambda)\exp\left(-\gamma_{BP}^T t\right). \tag{3-8}$$

Evaluating this expression at two different time instants t_1 and t_2, and then solving the resulting system simultaneously for the unknown spectra, we obtain

$$A_L(\lambda) = A_B(\lambda) + \frac{A(\lambda;t_2)\exp\left(\gamma_{BP}^T t_2\right) - A(\lambda;t_1)\exp\left(\gamma_{BP}^T t_1\right) - A_B(\lambda)\left[\exp\left(\gamma_{BP}^T t_2\right) - \exp\left(\gamma_{BP}^T t_1\right)\right]}{n_L^{ss_0}\left\{\exp\left[\left(\gamma_{BP}^T - \gamma_{BL}^T\right)t_2\right] - \exp\left[\left(\gamma_{BP}^T - \gamma_{BL}^T\right)t_1\right]\right\}},$$

$$A_P(\lambda) = A_B(\lambda) + \frac{A(\lambda;t_2)\exp\left(\gamma_{BL}^T t_2\right) - A(\lambda;t_1)\exp\left(\gamma_{BL}^T t_1\right) - A_B(\lambda)\left[\exp\left(\gamma_{BL}^T t_2\right) - \exp\left(\gamma_{BL}^T t_1\right)\right]}{n_P^{ss_0}\left\{\exp\left[\left(\gamma_{BL}^T - \gamma_{BP}^T\right)t_2\right] - \exp\left[\left(\gamma_{BL}^T - \gamma_{BP}^T\right)t_1\right]\right\}}.$$

(3-9)

Now, the only unknown quantities in the above expressions are the quantum-efficiency ratios $\Phi_L(\lambda_0)$ and $\Phi_P(\lambda_0)$. As was done before, several inequalities such as

$$\begin{aligned} n_P^{ss_0} &> n_L^{ss_0} \\ A_P(\lambda_0) &< A_L(\lambda_0) \end{aligned} \qquad \text{(3-10}a\text{)}$$

$$\left.\begin{aligned} A_P(\lambda) &\geq 0 \\ A_L(\lambda) &\geq 0 \end{aligned}\right\} \quad \forall\lambda \qquad \text{(3-10}b\text{)}$$

$$\left.\begin{aligned} A_P(\lambda) &< A_B(\lambda) \\ A_L(\lambda) &< A_B(\lambda) \\ A_P(\lambda) &< A_L(\lambda) \end{aligned}\right\} \quad \forall\lambda \geq \lambda_{red} \qquad \text{(3-10}c\text{)}$$

can be imposed upon the calculated quantities in an effort to obtain some useful bounds on these parameters; here λ_{red}, somewhere between 570 nm and 600 nm, roughly marks the boundary of the red part of the spectrum. For the sake of brevity, however, we omit a detailed analysis at this point and defer the discussion of relevant results to the next subsection.

We close here by confirming a point made earlier: if the film is probed for $t \geq 0$ at a wavelength $\lambda_1 \neq \lambda_0$, then the absorbance vector in Eq. (3-4) would have to be evaluated at λ_1, essentially introducing two additional unknowns $A_L(\lambda_1)$ and $A_P(\lambda_1)$ into the subsequent

derivation, thus rendering our approach impracticable; hence the need for the pump and probe beams to be of the same wavelength, as asserted before.

C Experimental results

Data supporting the three-state hypothesis have already been presented and discussed above; what remains to be done is the recovery of the pure *L*-state absorption spectrum within the present context. Since the changes in probe absorbance seen in 670-nm and 690-nm pump–probe experiments are negligibly small (owing to insignificant steady-state *L* population and *L*-state absorbance at these wavelengths), reliable parameter extraction and accurate spectral recovery can only be done using 633-nm data, with which we shall deal exclusively here as well.

Eq. (3-4) provides an analytical expression for the absorbance seen by the probe beam as a function of time, and thus, by fitting the experimental data with two exponentials [cf. Fig. 5], we can readily obtain estimates for the unknown parameters appearing therein, namely the thermal lifetimes γ_{BL}^{T} and γ_{BP}^{T} and the absorbance changes $\Delta A_L(\lambda_0)$ and $\Delta A_P(\lambda_0)$ associated with the decay of the *L* and *P* states, respectively. Before proceeding further, we note from Eq. (3-9) that the connection between the pure-state spectra $A_L(\lambda)$ and $A_P(\lambda)$ and the unknown quantum-efficiency ratios $\Phi_L(\lambda_0)$ and $\Phi_P(\lambda_0)$ is provided via the population density expressions in Eq. (3-7). Specifically, we observe that $n_L^{ss_0}$ is actually a function of $1+\Phi_P(\lambda_0)$, and since it is plausible to expect that $\Phi_P(\lambda_0) \cong \Phi(\lambda_0)$ and $\Phi(\lambda_0) << 1$ at 633 nm [cf. Table 1], it follows that $A_L(\lambda)$ should depend only very weakly on $\Phi_P(\lambda_0)$; a similar reasoning holds for the dependence of $A_P(\lambda)$ on $\Phi_L(\lambda_0)$ as well, and these arguments are indeed found to be true when numerical values are substituted into Eq. (3-9).

This, then, allows us to regard $\Phi_P(\lambda_0)$ as known, and attempt to bound $\Phi_L(\lambda_0)$ accordingly; in fact, due to our inability to determine it more precisely, we shall simply take $\Phi_P(\lambda_0) = \Phi(\lambda_0)$ in the sequel, even though there should clearly be a slight difference in the value of ϕ_{PB} in the two- and three-state models. Eq. (3-10*a*) provides the extremely loose bounds $4.16 \cdot 10^{-4} < \Phi_L(\lambda_0) < 283.21$, whereas Eq. (3-10*b*) yields the considerably tighter window $0.0125 < \Phi_L(\lambda_0) < 20.331$. Finally, the third inequality in Eq. (3-10*c*) provides the lower bound $\Phi_L(\lambda_0) > 0.0160$, and we choose to adopt this as a typical value for the quantum-efficiency ratio of the 13–*cis* cycle,[19] once again our ultimate guide in this admittedly subjective selection process being the "visual" quality of the pure-state spectra obtained via Eq. (3-9) using these assumed values.

With all the essential quantities thus at hand, we turn to the evaluation of $A_L(\lambda)$ using the transient spectra for t_1 = 30 sec and t_2 = 5 min shown in Fig. 6; the somewhat noisy result (due to error accumulation in numerical computations), a spectrum centered roughly around 570 nm, is shown in Fig. 8. As a validation of the assumptions elucidated above, we also mention that $A_P(\lambda)$ obtained with Eq. (3-9) is essentially identical to the one recovered from the 633-nm steady-state absorption spectrum within the two-state formalism. Finally, the values (at 633 nm) of the various quantities pertaining to the three-state model are collected in Table 2, and are to be compared with the corresponding numbers for the two-state model given in Table 1.

D The lifetime issue

A discussion of the thermal lifetimes of the *L* and *P* states is finally in order. The initial thermal lifetimes $\tau_q \equiv \left(\gamma_{Bq}^T\right)^{-1}$ of the two unstable states $q = L, P$ can be estimated on the basis of

the theoretical model for the probe absorbance, given analytically in Eq. (3-4) and shown tailored to fit experimental data in Fig. 5. This yields the values shown in Table 2, which seem rather extraordinary at first glance.

We note initially that the *L*-state lifetime in the acidified BM solutions is known to be on the order of several milliseconds,[6,9–11] which is roughly three orders of magnitude shorter than seen here. One possible suspect for this conspicuous lifetime extension is the gelatin host within which the BR–D85N molecules are embedded for the fabrication of the films used in optical data storage and processing applications, which may serve to slow down the conformational changes in the molecular structure during the relaxation $K \rightarrow L \rightarrow B$.

A perhaps more intriguing observation is related to the *P*-state lifetime, which is known from practical experience to be much longer than found here; in fact, patterns recorded on BR–D85N films are retained for months in the laboratory, hence leading to the belief that the *P* state is nearly permanent.[20] This apparent paradox is resolved when we examine the long-term 633-nm pump–probe behavior shown in Fig. 9, which reveals that the absorbance increase due to *P*-state decay follows a seemingly power-law type trend, leveling off considerably faster in the long run than does the exponential time dependence implied by the molecular rate equations. (For purposes of comparison, the double-exponential fit shown in Fig. 5 extrapolates to an absorbance value of 1.519 after 20 hours, which is considerably higher than the actual value of about 1.215 observed in Fig. 9.)

A convincing hypothesis for this behavior may be based on the fact that the pump–probe measurements were performed on a rather large area on the film. It is entirely plausible, then, that due to variations in properties like the local pH and the gelatin and water concentrations, *P*-state molecules far enough apart within such an extended volume may exhibit notably different

decay dynamics. Consequently, instead of using a constant thermal decay rate γ_{BP}^{T} for all *P*-state molecules, we now treat this quantity as a random variable γ with a suitably chosen probability density function $p_{\Gamma}(\gamma)$ characterizing the statistics of the fluctuation in the value of γ_{BP}^{T} among the different *P*-state molecules within the bleached volume of the film. The expected time evolution of the *P*-state population density for $t \geq 0$ is then found as

$$\begin{aligned} \bar{n}_P(t) &= \int_0^\infty n_P(t) p_{\Gamma}(\gamma) \mathrm{d}\gamma \\ &= \int_0^\infty n_P^{ss_0} \exp(-\gamma t) p_{\Gamma}(\gamma) \mathrm{d}\gamma = n_P^{ss_0} \boldsymbol{M}_{\Gamma}(it), \end{aligned} \tag{3-11}$$

where $\boldsymbol{M}_{\Gamma}(\omega) = \int_0^\infty p_{\Gamma}(\gamma) \exp(i\omega\gamma) \mathrm{d}\gamma$ is the (generally complex-valued) characteristic function of γ. Although it would be difficult to determine the precise form of $p_{\Gamma}(\gamma)$, some rather general requirements can be readily imposed upon it, such as reality, unimodality, causality (i.e., $p_{\Gamma}(\gamma) = 0$ for $\gamma < 0$), and reality and positive semi-definiteness of $\boldsymbol{M}_{\Gamma}(it)$. Among the standard distribution functions,[21] only the gamma distribution $p_{\Gamma}(\gamma) = \frac{1}{\Gamma(\mu)} \left(\frac{\mu}{\bar{\gamma}}\right)^{\mu} \gamma^{\mu-1} \exp\left(-\frac{\mu}{\bar{\gamma}}\gamma\right)$ meets these criteria, and thus we obtain

$$\bar{n}_P(t) = n_P^{ss_0} \left(1 + \frac{\bar{\gamma}}{\mu} t\right)^{-\mu}. \tag{3-12}$$

Here $\bar{\gamma}$ and μ, the mean and the degrees of freedom of the distribution, are parameters at our disposal in obtaining a good fit to the experimental data. We note that with $\mu \to 0$, Eq. (3-12)

exhibits the desired negative-exponential and power-law behaviors for small and large *t*, respectively, and indeed provides an excellent overall fit for the transient behavior of the film absorbance, as shown in Fig. 9 for $\bar{\gamma} = 0.0011134$ and $\mu = 0.0030431$, which is impossible to achieve with any pair of negative exponentials.

Since the *P*-state population does not seem to decay exponentially, it is not possible, nor meaningful, to ascribe to it a $\frac{1}{e}$-type lifetime. In order to quantify the long-term stability of this state, we therefore turn to the difference spectra $\Delta A(\lambda;\tau) \equiv A(\lambda;\tau) - A(\lambda;0)$ shown in Fig. 10, measured following the 670-nm bleaching of the film, with $A(\lambda;0)$ actually taken 30 seconds after the pump beam was turned off (i.e., the spectrum labeled "670 nm" in Fig. 3). This figure clearly shows the decay of the *P*-state molecules back to the *B* state (bleach recovery), and based on this data it is estimated that less than 5% of the *P*-state molecules returned to the *B* state after 7 days.

More interestingly, Fig. 10 also reveals the emergence of yet another state whose absorbance is centered around 390 nm, namely the *Q* state known to be thermally accessible via the *P* state.[22] Although there is insufficient data to obtain an accurate pure *Q*-state spectrum, it is estimated that nearly 9% of the *P*-state molecules have transitioned into the *Q* state by the end of 7 days, thus bringing the total loss of *P*-state molecules within this time period to about 14%. With reference to Fig. 10, the *P*-state molecules were observed to decay back to the *B* state at an initially higher rate, producing only a negligible *Q*-state population by the end of the first day; however, this situation was seen to change with time as *Q*-state formation started to compete with bleach recovery, shifting the isosbestic point between the *B* and *P* states from 550 nm to 560 nm, with an isosbestic point between the *P* and *Q* states emerging around 425 nm.

This slow and nearly linear formation of *Q* state over time is thought to be responsible for

the optical irreversibility observed with BR–D85N films.[18] Specifically, during each delay (especially during the long ones) between spectral measurements after the film was bleached to steady state, a small but nonnegligible fraction of the molecules in the *P* state thermally decay to *Q* in the dark. The 442-nm source used to erase the film after each experiment does not entirely eliminate this residual *Q* formation, and therefore a certain amount of *Q*-state accumulation is inevitable over a long period of time, which translates into a net loss of photoactive material from the photocycle and a fatigue of the film. We note parenthetically that a species with a 455-nm absorption peak observed in other BM forms of BR was not detected here;[5,13] it is unknown whether the absence of this intermediate is inherent to D85N, is due to the hydrated gelatin host, or was brought about by the particular experimental conditions of this study.

Before closing, we finally tie one last loose end by checking the accuracy of our earlier assumption that the thermal decay rates of the *L* and *P* states are much smaller than the concomitant photochemical transition rates from these states back to the *B* state, and that they can therefore be neglected in analyzing the photo-bleaching of the film. Evaluating Eq. (2-1) using the *L*- and *P*-state absorption spectra calculated above, reverse-transition quantum efficiencies quoted in the literature ($\phi_{BL} \cong 0.94$, $\phi_{BP} \cong 8.8 \cdot 10^{-3}$),[7,11] and the optical intensity of the 633-nm excitation ($I \cong 50\ \mathrm{W/m^2}$), we find that γ_{BL}^{P} is approximately an order of magnitude larger than the initial thermal decay rate γ_{BL}^{T} corresponding to the $\frac{1}{e}$ lifetime shown in Table 2, and the corresponding rate parameters for the *P* state are found to be separated by roughly three orders of magnitude. It is therefore safe to say that the assumption $\gamma_{Bq}^{T} << \gamma_{Bq}^{P}$ holds indeed.

We mention in passing that, given the complexity of the BR molecule, a theoretical calculation of the *P*-state lifetime as a function of ambient temperature would be a formidable analytical task, but this dependence can certainly be characterized empirically to assess the

"thermal ruggedness" of stored data. Perhaps all that can be said in this regard here is that the composition (and, in particular, the water content) of these films clearly precludes their use in extreme-temperature environments, and further that no change in BR–D85N photochemical response was detected in the narrow range of 20–30°C around room temperature.

4 Conclusion

In this paper, we presented a steady-state characterization of the photocycle of the photochromic material BR–D85N from the viewpoint of optical data storage and processing applications. Based on the simple two-state photocycle model $B \leftrightarrow P$ and steady-state bleach spectra, we were able to recover the pure P-state absorption spectrum, centered at 490 nm, and estimate the ratio $\Phi(\lambda)$ of the forward- and backward-transition quantum efficiencies of this cycle, all in remarkably good agreement with experimentally determined results reported elsewhere. It was seen in experiments, and also predicted by theory, that longer wavelengths in the red part of the spectrum populate the P state more efficiently; it is therefore clear that sources in the deep red should be used to obtain the highest possible absorption and index modulations with BR–D85N films. Of particular importance is the strong wavelength dependence of $\Phi(\lambda)$, which was seen to increase roughly linearly with increasing wavelength. This behavior is obviously essential to understanding the photochromism of BR–D85N, and seems to be overlooked in several articles in the BR literature.

In trying to assess the thermal stability of the P state, indications for the presence of an additional state in the photocycle were seen in pump–probe experiments. A bifurcated three-state photocycle model $L \leftrightarrow B \leftrightarrow P$ was then proposed and analyzed in light of the pump–probe absorbance data and time-resolved spectral measurements obtained from the steady-state-

bleached film, and we were thus able to reconstruct the pure *L*-state absorption spectrum, centered at 570 nm, within this context.

The *L* state seems to decay thermally within a matter of a few minutes entirely back to the *B* state. This observation has a potentially critical implication for data storage and processing: clearly, *L* is formed in regions of high recording-beam intensity where *P* is in fact intended to form; therefore, decay of *L* back to *B* after recording is complete essentially constitutes a degradation, or contamination, of stored information. Fortunately, as predicted theoretically and observed experimentally, the steady-state population density of the *L* state decreases as the excitation wavelength is moved deeper into the red part of the spectrum (e.g., less than 0.5% at 690 nm), which also achieves higher *P*-state populations as mentioned above, and therefore this data-contamination issue does not pose a serious problem.

The *P* state, on the other hand, was found to be relatively stable over time with a highly nonexponential decay behavior. A possible explanation for this was suggested to be the randomness in the decay characteristics of *P*-state molecules within an extended volume, which may also be problematic for data storage and processing applications as it implies a non-systematic data degradation that cannot be compensated for. If this randomness is in fact due to nonuniformities in the pH level and the water and gelatin content of the film, as suggested, then this problem can presumably be alleviated with careful film fabrication techniques.

For very long time delays, difference spectra revealed a thermal product of the *P* state, namely the *Q* state with an absorption spectrum centered around 390 nm (which could not be extracted accurately from available data), and the accumulation of this state over time presents yet another dilemma for data storage and processing as it amounts to a net loss of photoactive material as well as a degradation of recorded information. It is noted that for repeated

write–read–erase cycles, it is advisable to irradiate BR–D85N films with a wide-band blue source (e.g., filtered white light) to salvage as much of the BR molecules trapped in the *Q* state as possible. For long-term data storage, on the other hand, *Q*-state formation should be monitored periodically, and data should be retrieved or refreshed before the signal-to-noise ratio falls below an unacceptable level.

Finally, we mention that if this *Q*-state formation can be enhanced and accelerated by means of chemical or genetic engineering, then its presence in the BR–D85N photocycle may in fact be turned into an advantage: owing to a further separation of absorption bands, the $B \leftrightarrow Q$ photochromism would actually provide a larger absorption- and index-modulation depth,[2] which directly translates into a higher diffraction efficiency (i.e., signal-to-noise ratio) and an associated improvement in storage capacity for multiplexed holographic optical memories based on BR–D85N.

Acknowledgment

The authors would like to thank Prof. G. W. Rayfield of the University of Oregon for insightful discussions regarding the photocycle structure and kinetics of BR–D85N, and Dr. D. T. Smithey of Bend Research, Inc., for providing the BR–D85N films used in the experimental part of this work. All correspondence should be directed to the first author, who can be reached by phone at (650) 604-1262 and by e-mail at timucin@ptolemy.arc.nasa.gov.

References and Notes

1 See, for instance, R. R. Birge, "Nature of the primary photochemical events in rhodopsin and bacteriorhodopsin," Biochim. Biophys. Acta. **1016**, 293–327 (1990); R. R. Birge, "Photophysics and molecular electronic applications of the rhodopsins," Annu. Rev. Phys. Chem. **41**, 683–733 (1990); C. Bräuchle, N. Hampp, and D. Oesterhelt, "Optical applications of bacteriorhodopsin and its mutated variants," Adv. Mater. **3**, 420–428 (1991); D. Oesterhelt, C. Bräuchle, and N. Hampp, "Bacteriorhodopsin: a biological material for information processing," Q. Rev. Biophys. **24**, 425–478 (1991); J. K. Lanyi, "Proton translocation mechanism and energetics in the light-driven pump bacteriorhodopsin," Biochim. Biophys. Acta. **1183**, 241–261 (1993).

2 D. A. Timuçin and J. D. Downie, "Phenomenological theory of photochromic media: optical data storage and processing with bacteriorhodopsin films," J. Opt. Soc. Am. A **14**, 3285–3299 (1997).

3 See, for instance, T. Mogi, L. J. Stern, T. Marti, B. H. Chao, and H. G. Khorana, "Aspartic acid substitutions affect proton translocation by bacteriorhodopsin," Proc. Natl. Acad. Sci. USA **85**, 4148–4152 (1988); S. Subramaniam, T. Marti, and H. G. Khorana, "Protonation state of Asp (Glu)-85 regulates the purple-to-blue transition in bacteriorhodopsin mutants Arg-82 → Ala and Asp-85 → Glu: the blue form is inactive in proton translocation," Proc. Natl. Acad. Sci. USA **87**, 1013–1017 (1990); H. Otto, T. Marti, M. Holz, T. Mogi, L. J. Stern, F. Engel, H. G. Khorana, and M. P. Heyn, "Substitution of amino acids Asp-85, Asp-212, and Arg-82 in bacteriorhodopsin affects the proton release phase of the pump and the pK of the Schiff base," Proc. Natl. Acad. Sci. USA **87**, 1018–1022 (1990).

4 P. C. Mowery, R. H. Lozier, Q. Chae, Y.-W. Taeng, M. Taylor, and W. Stoeckenius, "Effect of acid pH on the absorption spectra and photoreactions of bacteriorhodopsin," Biochemistry **18**, 4100–4107 (1979).

5 A. Maeda, T. Iwasa, and T. Yoshizawa, "Formation of 9–*cis* and 11–*cis* retinal pigments

from bacteriorhodopsin by irradiating purple membrane in acid," Biochemistry **19**, 3825–3831 (1980).

6 H. Ohtani, T. Kobayashi, J.-I. Iwai, and A. Ikegami, "Picosecond and nanosecond spectroscopies of the photochemical cycles of acidified bacteriorhodopsin," Biochemistry **25**, 3356–3363 (1986).

7 S.-Y. Liu and T. G. Ebrey, "The quantum efficiency for the interconversion of the blue and pink forms of purple membrane," Photochem. Photobiol. **46**, 263–267 (1987).

8 C.-H. Chang, S.-Y. Liu, R. Jonas, and R. Govindjee, "The pink membrane: the stable photoproduct of deionized blue membrane," Biophys. J. **52**, 617–623 (1987).

9 G. Váró and J. K. Lanyi, "Photoreactions of bacteriorhodopsin at acid pH," Biophys. J. **56**, 1143–1151 (1989).

10 T. E. Thorgeirsson, S. J. Milder, L. J. W. Miercke, M. C. Betlach, R. F. Shand, R. M. Stroud, and D. S. Kliger, "Effects of Asp-96 → Asn, Asp-85 → Asn, and Arg-82 → Gln single-site substitutions on the photocycle of bacteriorhodopsin," Biochemistry **30**, 9133–9142 (1991).

11 J. K. Lanyi, J. Tiggor, G. Váró, G. Krippahl, and D. Oesterhelt, "Influence of the size and protonation state of acidic residue 85 on the absorption spectrum and photoreaction of the bacteriorhodopsin chromophore," Biochim. Biophys. Acta. **1099**, 102–110 (1992).

12 S. L. Logunov, M. A. El-Sayed, L. Song, and J. K. Lanyi, "Photoisomerization quantum yield and apparent energy content of the K intermediate in the photocycles of bacteriorhodopsin, its mutants D85N, R82Q, and D212N, and deionized blue bacteriorhodopsin," J. Phys. Chem. **100**, 2391–2398 (1996).

13 J. R. Tallent, J. A. Stuart, Q. W. Song, E. J. Schmidt, C. H. Martin, and R. R. Birge, "Photochemistry in dried polymer films incorporating the deionized blue membrane form of bacteriorhodopsin," Biophys. J. **75**, 1619–1634 (1998).

14 See, for instance, O. Werner, B. Fischer, A. Lewis, and I. Nebenzahl, "Saturable absorption, wave mixing, and phase conjugation with bacteriorhodopsin," Opt. Lett. **15**, 1117–1119 (1990); R. Thoma, N. Hampp, C. Bräuchle, and D. Oesterhelt, "Bacteriorhodopsin films as

spatial light modulators for nonlinear-optical filtering," Opt. Lett. **16**, 651–653 (1991); D. Zeisel and N. Hampp, "Spectral relationship of light-induced refractive index and absorption changes in bacteriorhodopsin films containing wild-type BR_{WT} and the variant BR_{D96N}," J. Phys. Chem. **96**, 7788–7792 (1992); Q. W. Song, C. Zhang, R. Blumer, R. B. Gross, Z. Chen, and R. R. Birge, "Chemically enhanced bacteriorhodopsin thin-film spatial light modulator," Opt. Lett. **18**, 1373–1375 (1993).

15 All absorption spectra shown in this paper were obtained with a Shimadzu UV-2501PC UV-VIS Recording Spectrophotometer.

16 See, for instance, R. A. Mathies, C. H. Brito Cruz, W. T. Pollard, and C. V. Shank, "Direct observation of the femtosecond excited-state *cis–trans* isomerization in bacteriorhodopsin," Science **240**, 777–779 (1988); M Rohr, W. Gärtner, G. Schweitzer, A. R. Holzwarth, and S. E. Braslavsky, "Quantum yields of the photochromic equilibrium between bacteriorhodopsin and its bathointermediate K. Femto- and nanosecond optoacoustic spectroscopy," J. Phys. Chem. **96**, 6055–6061 (1992); S. L. Logunov, L. Song, and M. A. El-Sayed, "pH dependence of the rate and quantum yield of the retinal photoisomerization in bacteriorhodopsin," J. Phys. Chem. **98**, 10674–10677 (1994); K. C. Hasson, F. Gai, and P. A. Anfinrud, "The photoisomerization of retinal in bacteriorhodopsin: experimental evidence for a three-state model," Proc. Natl. Acad. Sci. USA **93**, 15124–15129 (1996); F. Gai, K. C. Hasson, J. C. McDonald, and P. A. Anfinrud, "Chemical dynamics in proteins: the photoisomerization of retinal in bacteriorhodopsin," Science **279**, 1886–1891 (1998).

17 Due to the insensitivity of BR–D85N, a large pump fluence is required to bleach the film to steady-state conditions (e.g., of the order of a few hundred J/cm^2 for 633-nm excitation). Clearly, this energy can be delivered within a short time period by using a powerful source; however, this presents the danger of denaturing the protein due to excessive heat dissipation,[13] which would lead to a (highly undesirable) loss of photoactive material. In our experiments, we therefore used relatively weak pump beams to ensure adiabatic bleaching of the material.

18 Perhaps the most direct evidence for this would be the failure of the absorption spectra of the bleached film in forming a perfect isosbestic point, and close inspection of the 520–540 nm region in Figs. 2, 3, and 6 indeed reveals that the bleached spectra do not intersect the *B*-state spectrum at a single point, as they would for a truly two-state photocycle. This, however, can also be due to (1) a type of irreversibility (or "fatigue") whereby erasure between exposure with different wavelengths does not return the film to the same initial state, or (2) the thermal denaturation of the protein upon continuous high-power exposure. (Incidentally, the former is actually the case here, as discussed in the text.[17]) The lack of an isosbestic point, therefore, does not by itself provide conclusive evidence for the inadequacy of the two-state model.

19 Since ϕ_{KB} is roughly 0.1 at $\lambda_0 = 633$ nm while ϕ_{BL} is nearly unity, this low value of $\Phi_L(\lambda_0)$ indicates a strong photochemical back-conversion $K \rightarrow B$ in the 13–*cis* cycle, which is consistent with the fact that the *K* state, with a spectrum centered around 640 nm, absorbs prominently in the red.[6–12]

20 In aqueous films with no chemical cross-linking between the BR molecules and the host matrix, optically recorded information "fades" due to molecular diffusion: BR molecules spatially arranged into different states by the recording beams subsequently migrate to attain uniform population densities throughout the film volume, causing the loss of recorded information in the process; see J. D. Downie, D. A. Timuçin, D. T. Smithey, and M. Crew, "Long holographic lifetimes in bacteriorhodopsin films," Opt. Lett. **23**, 730–732 (1998). This, of course, is of no consequence in PM (wild-type and D96N) BR films where *M*-state molecules quickly decay back to the *B* state before appreciable diffusion can take place. In the present case, however, since the sample under study is a large and uniformly bleached portion of the film (i.e., no spatial variation in the initial molecular population densities), diffusion effects cannot be responsible for the change in film absorbance observed over the time scales of interest here.

21 A. Papoulis, *Probability, Random Variables, and Stochastic Processes*, 3rd ed. (McGraw-Hill, New York, 1991).

22 A. Popp, M. Wolperdinger, N. Hampp, C. Bräuchle, and D. Oesterhelt, “Photochemical conversion of the O-intermediate to 9–*cis*-retinal-containing products in bacteriorhodopsin films,” Biophys. J. **65**, 1449–1459 (1993).

Table Captions

1 Ratio of the forward- to backward-transition quantum efficiencies and the steady-state population densities as a function of the bleaching wavelength in the two-state photocycle model of BR– D85N. [a] Obtained using Eq. (2-9). [b] Obtained using Eq. (2-10). [c] See text for explanation. [d] Obtained using Eq. (2-5) and $n_P = 1 - n_B$.

2 Ratio of the forward- to backward-transition quantum efficiencies and the steady-state population densities for λ_0 = 633 nm excitation in the three-state photocycle model of BR–D85N. [a] See text for explanation. [b] Obtained using Eq. (3-7) and $n_B = 1 - n_L - n_P$. [c] Based on the theoretical fit via Eq. (3-4) shown in Fig. 5.

Bleaching wavelength		Quantum-efficiency ratio [$\Phi(\lambda_0)$]			Steady-state population densities [d]	
λ_0 (nm)	λ_1 (nm)	Lower bound [a]	Upper bound [b]	Typical value [c]	*B* state [$n_B^{ss_0}$]	*P* state [$n_P^{ss_0}$]
633	670	0.0018	0.2906	0.0180	0.4854	0.5146
	690		0.0991			
670	690	0.0045	0.7878	0.0594	0.1845	0.8155
690	—	0.0491	∞	0.2453	0.0826	0.9174

Table 1

Quantity		Typical Value
Quantum-efficiency ratios [a]	9–*cis* cycle	$\Phi_P(\lambda_0) = 0.0180$
	13–*cis* cycle	$\Phi_L(\lambda_0) = 0.0160$
Steady-state population densities [b]	*B* state	$n_B^{ss_0} = 0.4733$
	L state	$n_L^{ss_0} = 0.0191$
	P state	$n_P^{ss_0} = 0.5076$
Initial thermal lifetimes [c]	*L* state	$\tau_L \cong 1$ min
	P state	$\tau_P \cong 2.5$ days

Table 2

Figure Captions

1 Two-state photocycle model for BR–D85N.

2 Measured absorption spectrum of the *B* state.

3 Mixed absorption spectra of the film in steady state for three bleaching wavelengths; isosbestic-point wavelength $\lambda_{iso} \cong 530$ nm.

4 Calculated absorption spectrum of the *P* state.

5 Pump($t < 0$)–probe($t \geq 0$) absorbance data at 633 nm; the theoretical fit employs two exponentials corresponding to the thermal decay of the *L*- and *P*-state molecules.

6 Transient absorption spectra of the 633-nm bleached film for three time instants; bleaching beam was turned off at $t = 0$.

7 Three-state photocycle model for BR–D85N.

8 Calculated absorption spectrum of the *L* state.

9 Long-term pump–probe absorbance data at 633 nm; the theoretical fit incorporates the (postulated) randomness in the thermal decay rate of the *P*-state molecules.

10 Difference absorption spectra of the 670-nm bleached film, showing the long-term depletion of the *P* state into the *B* and *Q* states.

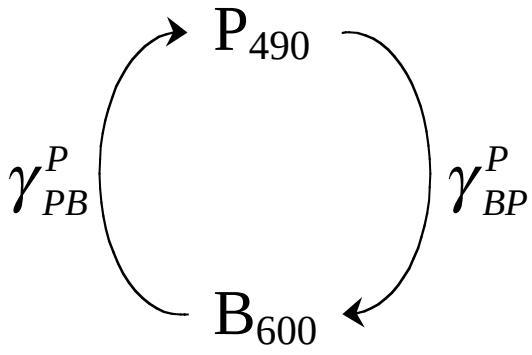

Figure 1

D. A. Timuçin

Journal of the Optical Society of America B

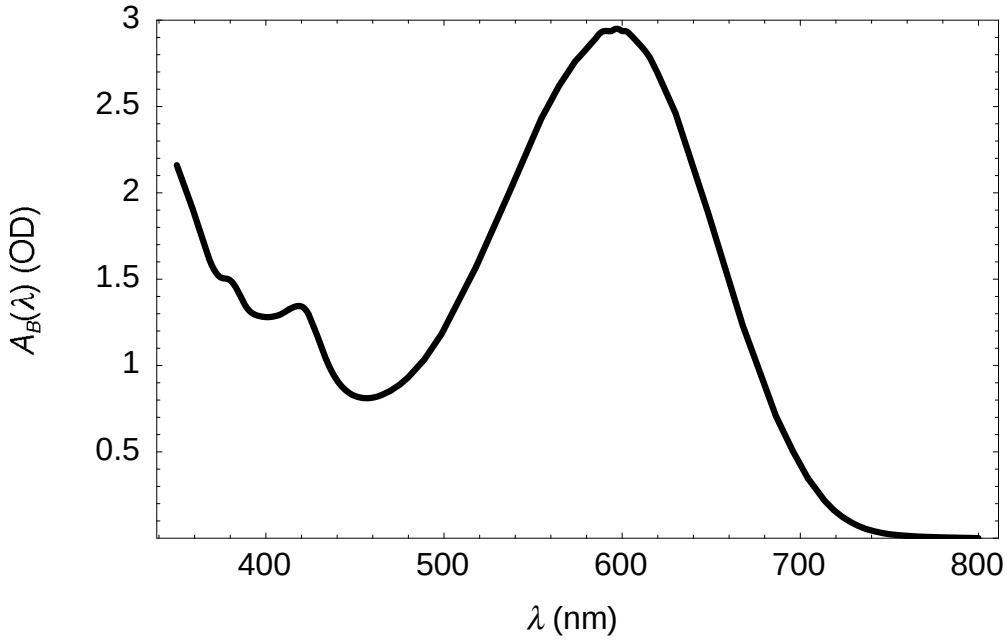

Figure 2

D. A. Timuçin

Journal of the Optical Society of America B

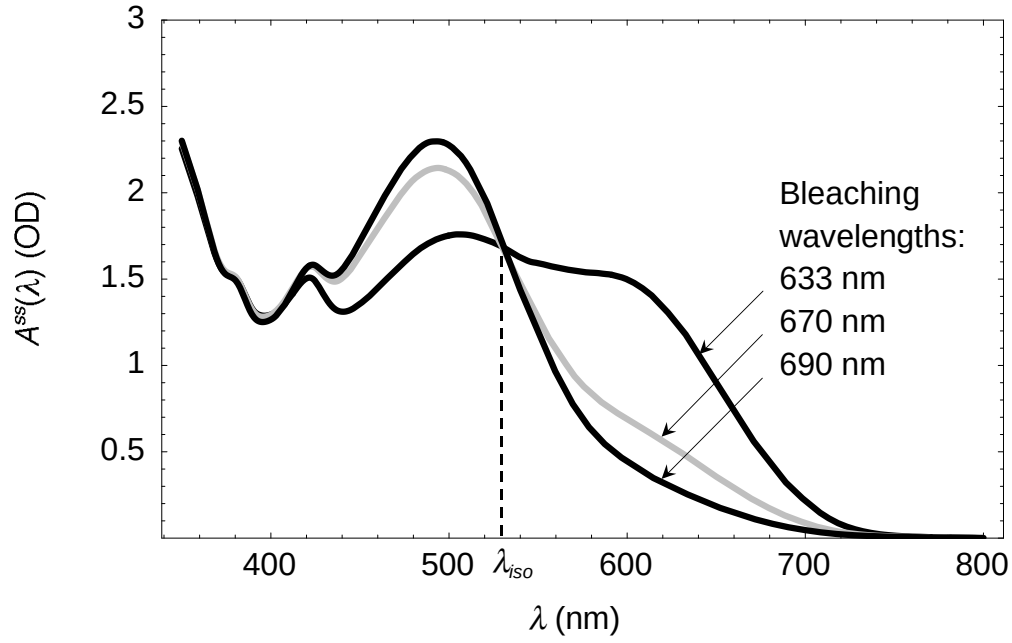

Figure 3

D. A. Timuçin

Journal of the Optical Society of America B

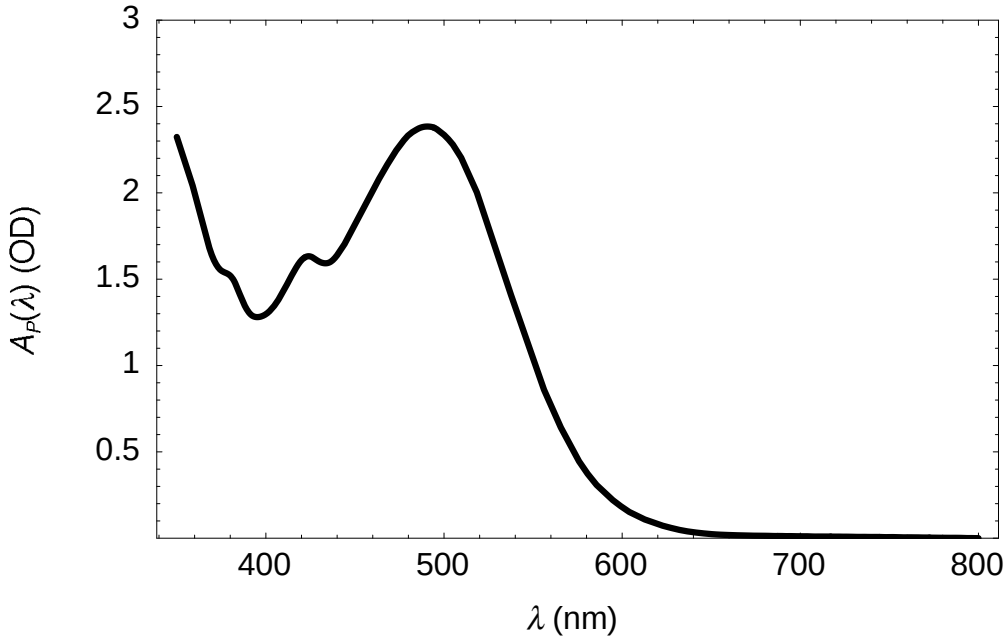

Figure 4

D. A. Timuçin

Journal of the Optical Society of America B

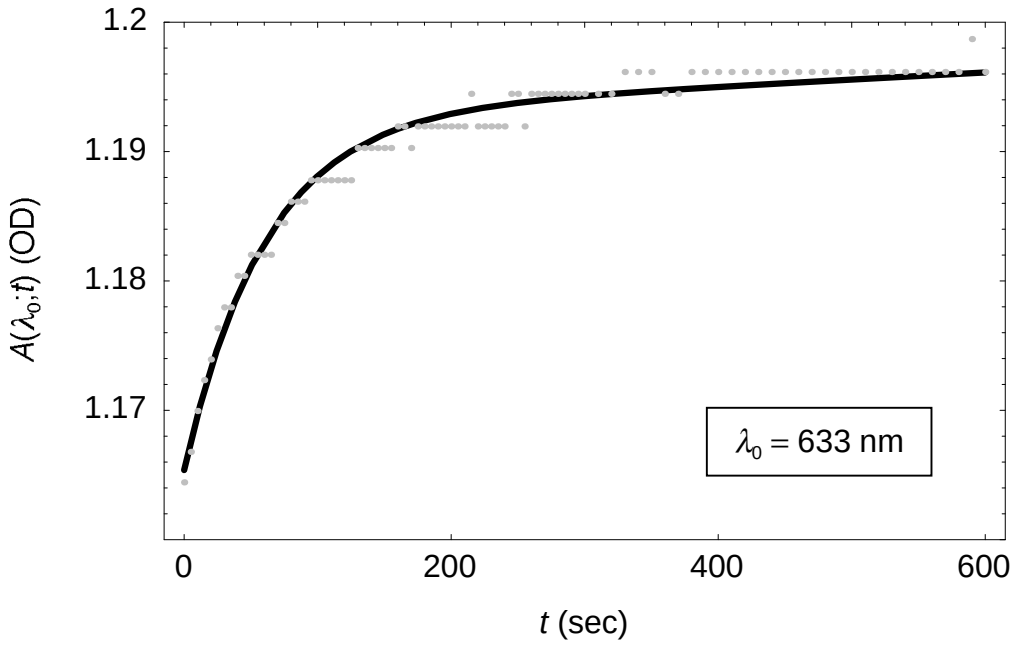

Figure 5

D. A. Timuçin

Journal of the Optical Society of America B

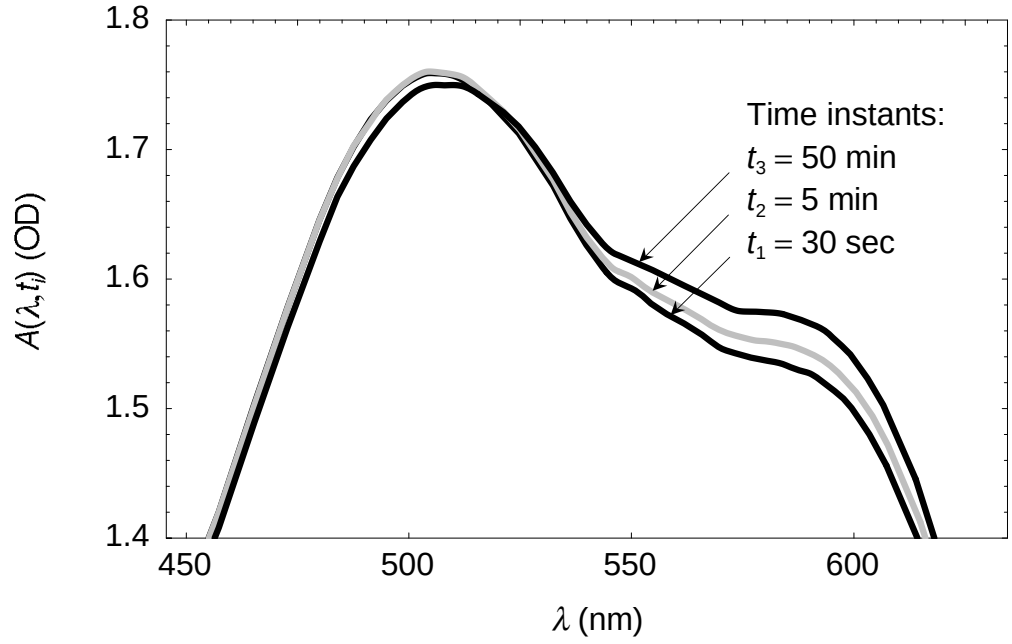

Figure 6

D. A. Timuçin

Journal of the Optical Society of America B

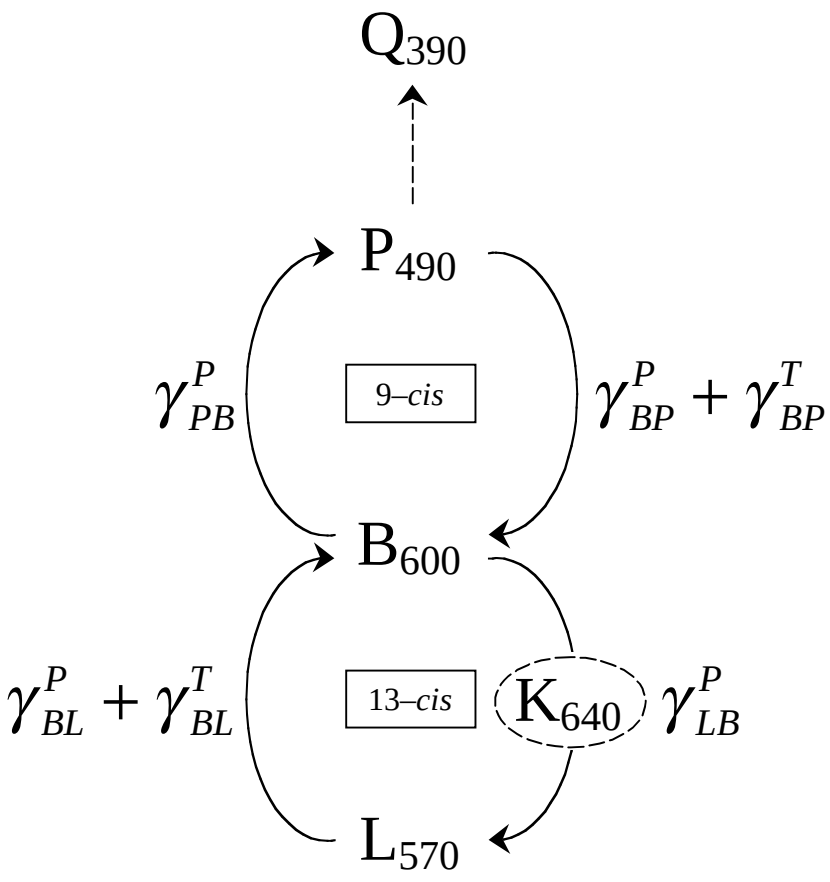

Figure 7

D. A. Timuçin

Journal of the Optical Society of America B

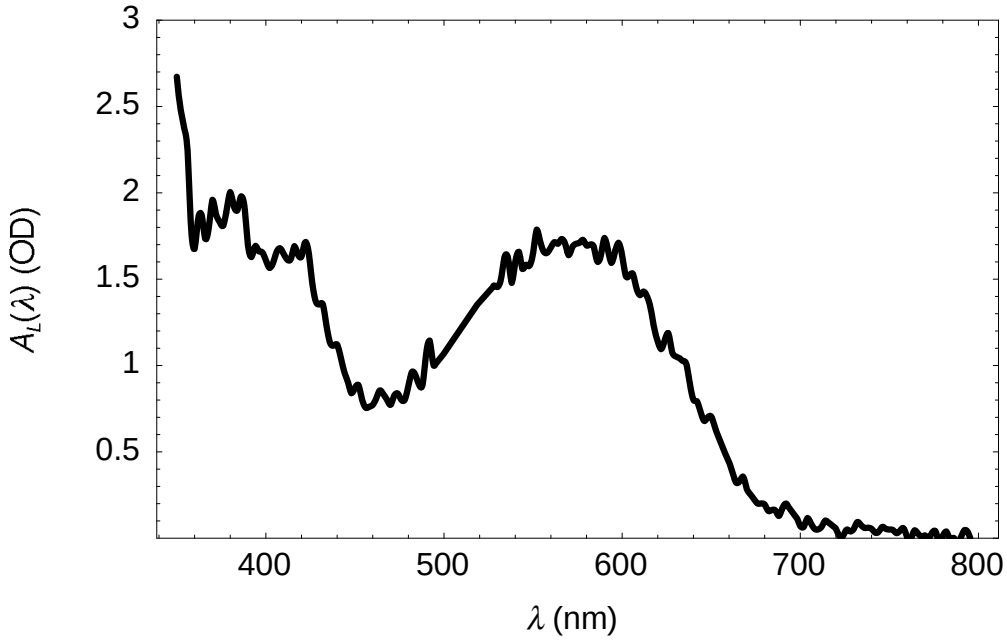

Figure 8

D. A. Timuçin

Journal of the Optical Society of America B

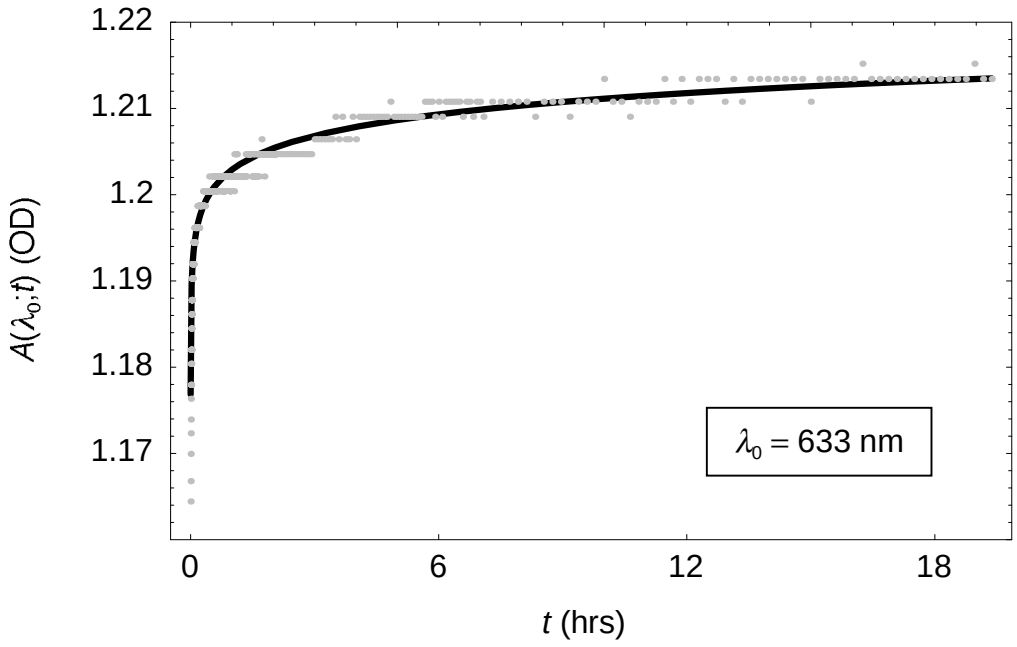

Figure 9

D. A. Timuçin

Journal of the Optical Society of America B

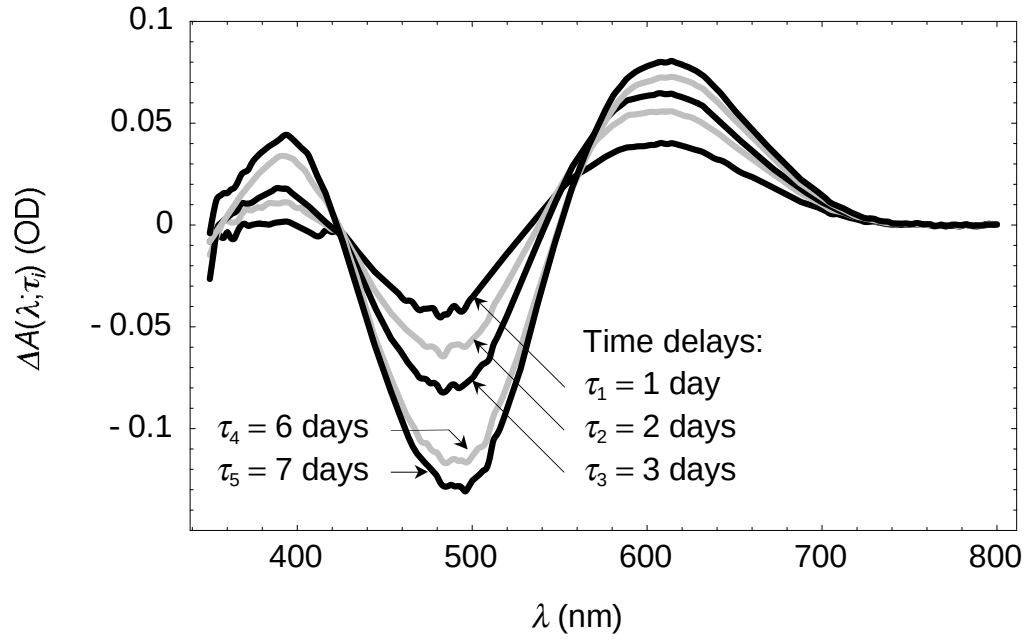

Figure 10

D. A. Timuçin

Journal of the Optical Society of America B